

# Carbonation and Leaching Behaviors of Cement-Free Monoliths Based on High-Sulfur Fly Ashes with the Incorporation of Amorphous Calcium Aluminate

Mustafa Cem Usta,\* Can Rüstü Yörük, Mai Uibu, Reiner Traksmäa, Tiina Hain, Andre Gregor, and Andres Trikkel



Cite This: *ACS Omega* 2023, 8, 29543–29557



Read Online

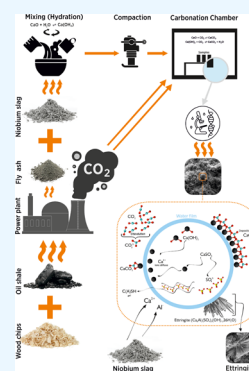
ACCESS |

Metrics & More

Article Recommendations

Supporting Information

**ABSTRACT:** The high sulfate content in various alkaline wastes, including those from fossil fuel and biomass combustion, and other industrial processes, necessitates careful management when used in cementitious systems to prevent potential deterioration of construction materials and environmental safety concerns. This study explores the under-researched area of high-sulfur fly ash (HSFA) utilization in the production of cement-free monoliths through accelerated carbonation and further examines the effect of niobium slag (NS)—a calcium aluminate-containing slag—as an additive on the strength development and the mobility of  $\text{SO}_4^{2-}$ . The methodology involves mineralogical and microstructural analyses of monoliths before and after carbonation, accounting for the effects of accelerated carbonation treatment and NS addition. The findings suggest that accelerated carbonation significantly improves the initial compressive strength of the HSFA monoliths and generally immobilizes heavy metals, while the effect on sulfate immobilization can vary depending on the ash composition. Moreover, the addition of NS further enhances strength without substantially hindering  $\text{CO}_2$  uptake, while reducing the leaching values, particularly of sulfates and heavy metals. These findings suggest that it is feasible to use calcium aluminate-containing NS in HSFA-based carbonated monoliths to immobilize sulfates without compromising the strength development derived from carbonation. This research contributes to the understanding of how accelerated carbonation and NS addition can enhance the performance of HSFA-based materials, providing valuable insights for the development of sustainable construction materials.



## 1. INTRODUCTION

The recycling of industrial alkaline solid waste is a key aspect of sustainable development which reduces the demand for natural resources and contributes to a lowering of greenhouse emissions in construction products. Thus, the utilization of industrial waste or byproducts can play a significant role in the cleaner production of construction materials. Evaluating the integration of secondary resources from various industrial sources is crucial to ensure these new materials meet the necessary technological and environmental standards. The quality of the potential supplementary cementitious materials can be evaluated with the chemical and mineralogical compositions of industrial wastes through various regulations and standards.<sup>1–3</sup> Fly ashes (FA) are widely known and utilized as supplementary and alternative cementitious materials.<sup>4,5</sup> Yet FA particle is only a few microns in thickness and can contain leachable toxic heavy metals and salts, which can limit the possibilities for the valorization of these materials. The  $\text{SO}_3$  content in fly ashes (FAs) is a critical parameter, especially in high-sulfur fly ashes (HSFA), as a high sulfur content can lead to various adverse effects such as sulfate attack and reduced durability in cementitious systems.<sup>6,7</sup> These potential issues can significantly limit the utilization and applications of HSFA, despite its wide availability. Recycling of

FAs or other types of out-of-furnace byproducts with high sulfur content<sup>8–11</sup> as supplementary cementitious materials requires compliance with legal standards,<sup>12</sup> which can be complex and costly once the sulfur removal treatments are considered.<sup>13</sup> Ashes from different fossil fuel (coal, oil shale, etc.) combustion processes as well as ashes of biomasses (wood, forestry waste, etc.), flue gas desulfurization waste, construction demolition wastes, slags from metal smelting, pulp, and paper mill waste, etc. can contain high amounts of sulfate.<sup>14–21</sup> Therefore, the utilization of these types of wastes especially HSFA in cementitious systems requires careful consideration and management to ensure that the negative effects of the high sulfur content are minimized for potential problems regarding deterioration and environmental safety of construction materials. Reduction of hazardous characteristics can be achieved using appropriate mix designs, washing

Received: May 16, 2023

Accepted: July 5, 2023

Published: July 31, 2023



techniques,<sup>22,23</sup> or the incorporation of additives such as hydraulic binders, i.e., amorphous calcium aluminate (CA).<sup>8,24–26</sup> Trincal et al. tested various experimental binders for their effectiveness in reducing sulfate leaching from soils with high gypsum content (maximum of 34 wt %).<sup>27</sup> The researchers found that the formation of ettringite partially immobilized the sulfates. The most successful binder was a hydraulic mixture consisting mainly of ye'elimite (C<sub>4</sub>A<sub>3</sub>S̄) and belite (C<sub>2</sub>S), which decreased the leachable sulfate concentration by 50% in leaching tests. Further, Sadique et al.<sup>28</sup> investigated the hydration mechanism of a non-Portland binder (wastepaper sludge ash); during sulfate activation, demonstrating that the alumina phase in the ash reacts with the elevated SO<sub>4</sub><sup>2-</sup> concentration to produce aluminosulfate, which mixes with Ca<sup>2+</sup> to create ettringite.

CAs, and by extension the calcium sulfoaluminate (CAS) phases are known to be rapidly reactive hydraulic compounds that improve the strength of hardened mortars.<sup>29</sup> A major advantage of calcium sulfoaluminate phases or ettringite-based chemistry, as applied to the stabilization of residues, is the extremely low solubility of ettringite at alkaline pHs in the range of 10.4–13.7, thereby providing strong resistance to sulfate leaching.<sup>30,31</sup> The studies conducted by Rungchet et al. and Mrak et al. showed that the leaching of heavy metals and sulfates can be controlled via calcium sulfoaluminate phases<sup>32,33</sup> and similarly, Luo et al.<sup>34</sup> have found that sulfoaluminate cement can also effectively decrease the toxic leaching of heavy metals.

Recent research has pivoted toward accelerated carbonation of industrial alkaline wastes, a process that recycles carbon dioxide and reduces hazardous compounds.<sup>35</sup> This approach enhances the use of these wastes as alternative cementitious materials, fostering the creation of eco-friendly construction products and promoting a circular economy within the construction sector.<sup>36,37</sup> Experimental results have proven that the accelerated carbonation process improves the mechanical properties of the different test specimens (monoliths, pastes, granules, etc.) by altering physical characteristics like porosity and surface area.<sup>38</sup> Besides, the accelerated carbonation process lowers the mobility of hazardous compounds, encapsulating the toxic substance into the structure of the final product. Hence, stabilization of the industrial alkaline solid wastes can be achieved through accelerated carbonation, by creating stable precipitates that are insoluble to reduce the leachability of potentially harmful elements.<sup>39–41</sup> Lange et al. studied the leaching characteristics of cement-solidified waste forms upon carbonation.<sup>42</sup> Results showed that the carbonated solidified products had mean strength values increased by up to 70% and leachable metal concentrations reduced by up to 80%. Baciocchi et al. investigated the leaching behavior of refused derived fuel bottom ash through the accelerated carbonation method and concluded that a significant reduction of the mobility of most contaminants can be achieved.<sup>38</sup> However, studies regarding FAs in this field are rather limited, especially the utilization of HSFAs through accelerated carbonation in the construction industry remains understudied. Furthermore, a method of application incorporating accelerated carbonation can be challenging for HSFAs as the literature is rather ambiguous, and different leaching outcomes have been reported for the carbonation process in the past. Bergmans et al. found that as the pH of the leachate decreases, the sulfate concentration in the solution increases.<sup>43</sup> This pH-dependent behavior in

sulfate leaching is consistent with the solubility of ettringite. Wang et al. concluded that there is no obvious correlation between reactivity during the carbonation of FA and the concentration of leachable sulfate, and the carbonation process did not influence the level of sulfates.<sup>44</sup> Li et al. however, claim that the release of soluble salts including SO<sub>4</sub><sup>2-</sup> was reduced by the carbonation of FA.<sup>45</sup>

Therefore, the main objectives of this study are; first to evaluate the carbonation potential of oil shale FA and wood FA as targeted HSFAs materials in carbonated structures for cement-free building material applications, second to characterize the sulfate leaching behavior of these cement-free monoliths and finally to investigate the effects of niobium slag as an additive to HSFAs for the evaluation of its role in possible immobilization of SO<sub>4</sub><sup>2-</sup> and strength development in carbonated structures. This approach significantly deviates from conventional practices and has not been thoroughly investigated in prior research. A distinctive innovation of this study is the incorporation of niobium slag, a material enriched with amorphous CA, as an additive to HSFAs, that could potentially augment the performance and sustainability of HSFAs-based materials in the construction sector.

In essence, the significance of this study lies in the novel exploration of accelerated carbonation of HSFAs with a slag-based calcium aluminate additive.

## 2. MATERIALS AND METHODS

**2.1. Materials.** Three different types of industrial by-product samples (namely, oil shale fly ash (OSFA), wood fly ash (WFA), and niobium slag (NS)) were selected from the power and heat generation and metal sectors of Estonia, which represents the widely available low-grade fuel operated circulating fluidized bed (CFB) combustion residues as well as co-firing applications with biomass elsewhere. OSFA was obtained from Auvere Power Plant,<sup>46</sup> which is primarily operated by the direct combustion of OS with the ability to co-fire with up to 50% woodchips in CFB boilers for power production, and ash was collected from the electrostatic precipitators. WFA was obtained from AS Utilitas Tallinn,<sup>47</sup> which has a biofuel-based combined heat and power station supplied by mainly waste forestry wood and ash was collected from bag filters located in the postcombustion zones of the grate combustor. Calcium aluminate-bearing NS (as ground sample) is obtained from NPM Silmet. One of Europe's leading producers of rare metals (annual output of 700 t) and rare earth metals (annual production of 3000 tons) is NPM Silmet.<sup>48</sup> Niobium slag produced by the metallurgical process now amounts to 1000 tons or more annually. The major byproducts of the calcium aluminothermic reduction of niobium oxide (Nb<sub>2</sub>O<sub>5</sub>) are mostly calcium aluminate-containing slag and pure Nb. Niobium oxide Nb<sub>2</sub>O<sub>5</sub> (3–7%) and pure Ni (perhaps up to 1%) remain in slag because of the non-full calcium aluminothermic reduction.<sup>49</sup>









**2.2. Characterization of Materials and Methods.** Mean samples were taken from each collected residue and a size fraction below 200 μm (by sieving) was used for material characterization and further sample preparation. The physical characterization of the selected waste streams included particle size distribution (PSD) measurements. Horiba Laser Scattering instrument (LA-950V2) was used for PSD measurement (with ethanol as a dispersant). The BET-N<sub>2</sub> sorption method was used to measure the specific surface area (SSA) with a Kelvin 1042 sorptometer (Costech Microanalytical SC). Helium was

used as a carrier gas, while N<sub>2</sub> (purity 99.999%) was used as an adsorptive gas. N<sub>2</sub> adsorption data were collected at relative pressures ( $p/p_0$ ) ranging from 0.05 to 0.2 at the liquid N<sub>2</sub> temperature of  $-196.15\text{ }^\circ\text{C}$ . The SSA was calculated based on Brunauer–Emmett–Teller (BET) theory. The content of free lime and carbon (ELTRA CS 580 Carbon Sulfur Determinator) was determined in the solid phase. Pore size distribution and porosity measurements were obtained through a Mercury intrusion porosimeter (MIP) using a POREMASTER-60-17 porosimeter (Quantachrome Instruments). The total porosity was calculated by dividing the complete volume of mercury infiltrated at the highest experimental pressure by the overall volume of the sample being tested. The porosity measurements were performed at least twice and occasionally three times to ensure repeatability. The chemical and mineralogical characterization as well as the phase changes after different curing steps of the selected waste streams were analyzed by X-ray fluorescence (XRF) (Bruker S4 Pioneer) and X-ray diffraction (XRD) with Rigaku, SmartLab SE. The X-ray tube uses a Cu anode (wavelength 1.5406 Å). D/teX Ultra 250 1D detector was used for measurement. The measuring range was  $9\text{--}60^\circ$ , the step length was  $0.04^\circ$ , and the measuring speed was  $3^\circ/\text{min}$ . The ICDD PDF4 database was used for data processing. The thermogravimetric (TGA) analysis was also carried out to understand the thermal characterization of both carbonated and uncarbonated monoliths (mainly for the calculation of CO<sub>2</sub> uptake) by using a Setaram Labsys 2000 thermoanalyzer (10 K/min, sample mass:  $20 \pm 1\text{ mg}$ , 21% O<sub>2</sub>/79% Ar) with alumina (Al<sub>2</sub>O<sub>3</sub>) crucible. The microstructures of the carbonated samples were analyzed by a scanning electron microscope (SEM) ZEISS Evo MA 15 with an EDX analyzer. The compressive strength measurements were performed with Toni TechnikD-13355.

Leaching tests were applied first to the initial ashes and later to both uncarbonated (UC) and carbonated (C) samples with NS additive according to the standard EN 12457-2. Crushed pieces were taken from initially hardened samples and were kept in sealed centrifuge tubes with distilled water for  $24 \pm 0.5\text{ h}$  in an overhead shaker (GFL 3025) with 34 rpm rotation speed at room temperature ( $20 \pm 2\text{ }^\circ\text{C}$ ). The liquid-to-solid ratio (L/S) was 10 L/kg and the grain size of the crushed monoliths was between 0 and 4 mm. Later the suspension was vacuum filtered (standard filter paper, pore diameter  $0.45\text{ }\mu\text{m}$ ). Conductivity (EC) and pH values were measured using a Mettler Toledo SevenGo Duo Pro pH/Cond meter SG23. Cl<sup>-</sup> and SO<sub>4</sub><sup>2-</sup> ions were determined through Lovibond Spectro direct spectrometer, silver nitrate turbidity, and barium sulfate turbidity methods, respectively. The Agilent 4210 Microwave Plasma Atomic Emission Spectrometer (MP-AES) with nitrogen-based plasma generated from magnetically coupled microwave energy was used for the determination of heavy metals (Ba, Cr, Cu, Fe, Ni, Pb, Sr, Zn, Mn, Cd, etc.).

**2.2.1. Sample Preparation and Experimental Setup.** Samples are prepared in four different compositions including 100% OSFA, 100% WFA and 10% NS added to both OSFA and WFA (see Table 1). Each batch of samples included a minimum of four cylindrical samples and their average strength values are given in the results for each tested parameter. In the first step, the hydrated OSFA and WFA samples have been prepared with a liquid-to-solid ratio of 0.20 w/v. The moisture content has been measured using an MB23 moisture analyzer. The semibatch Eirich EL1 type intensive mixer was used for mixing. The samples were homogeneously mixed with

**Table 1. Labeling of Monolithic Specimens (UC: Uncarbonated, C: Carbonated)**

Composition	UC	C
OSFA (100%)	 x 4	 x 4
WFA (100%)	 x 4	 x 4
90% OSFA + 10% NS	 x 4	 x 4
90% WFA + 10% NS	 x 4	 x 4

deionized water at the fixed rotation speed (600 rpm) and time (20 min). Later, the samples were left to hydrate/cure in sealed and vacuumed containers at room temperature ( $10 \pm 0.5\text{ h}$ ) and were compacted in the next step using a hydraulic press into cylinders with a diameter of 20 mm and height of  $20 \pm 1\text{ mm}$ .

NS (10 wt %) was incorporated into samples in a dry form after the first hydration period of ash samples and mixed for a fixed time (10 min) as calcium aluminate-bearing slags cause rapid hydration and hardening, which do not allow for a long waiting period before press forming. As press molding of samples was carried out with a manual (hand-operated) hydraulic press, serious attention was given to the uniform preparation of samples. NS powder has lower compressibility compared to the ash samples which affects the compaction ability of the sample based on the ratio of mix. The optimum compaction pressure of  $300 \pm 10\text{ kg/cm}^2$  was selected based on the optimum workability, as lower compaction can result in low rigidity and effects the green strength of the samples before carbonation while higher compaction can inhibit carbonation as samples become less porous. Carbonation experiments were performed in an automated carbonation unit (stainless-steel 400 mL jacketed pressure vessel), consisting of apparatus controlling temperature (Circulator C-400). Furthermore, the carbonation experiments tests were performed under a controlled humidity environment using a potassium iodide saturated solution, which inhibits excessive humid conditions and maintains a relative humidity between 60 and 70% at room temperature. The optimum curing parameters (5 bar, 100% CO<sub>2</sub>,  $25\text{ }^\circ\text{C}$ , 4 h) were selected based on previously conducted parametric studies.<sup>5</sup>

Samples for MIP tests were prepared after the curing stage by taking crushed pieces up to  $5\text{ mm} \times 5\text{ mm} \times 5\text{ mm}$  from inside and outside the cylindrical samples making the selection as homogeneous as possible. To stop the hydration, these pieces were twice submerged in ethanol for 24 h. The samples were dried in an oven at  $60\text{ }^\circ\text{C}$  after being treated with ethanol to remove the solvent.

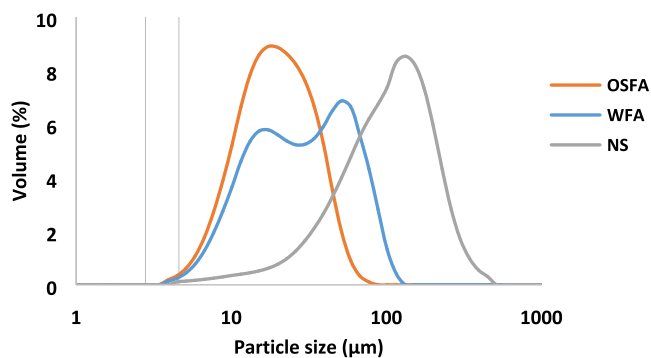
**2.2.2. Physical Characterization.** The carbonation efficiency and capacity tend to increase with decreasing particle size of fly ash due to two main reasons: first, smaller particles have a larger surface area which promotes carbonation reactions, and second, smaller particle size facilitates the release of metal ions such as Ca<sup>2+</sup> and Mg<sup>2+</sup>.<sup>50,51</sup> PSD analysis of samples indicated that OSFA with a mean particle size of  $17.97\text{ }\mu\text{m}$  has a smaller particle size compared to WFA, which has a mean particle size of  $26.84\text{ }\mu\text{m}$  (Table 1). However, the surface area of WFA is 3 times higher than OSFA (Table 2) due to the presence of unburned carbon which potentially plays a role in increasing the specific surface area by providing more active sites for chemical reactions and adsorption.<sup>51</sup> NS has a much higher mean particle size compared to FAs (Figure



**Table 2.**  $D_{10}$ ,  $D_{50}$ , and  $D_{90}$  Values of PSD and BET SSA of Samples

	$D_{10}$ ( $\mu\text{m}$ )	$D_{50}$ ( $\mu\text{m}$ )	$D_{90}$ ( $\mu\text{m}$ )	BET SSA ( $\text{m}^2/\text{g}$ )
OSFA	8.63	17.97	36.23	3.18
WFA	9.65	26.84	65.68	9.81
NS	33.61	99.87	204.38	0.34

1) with lower SSA due to its high-temperature production process, which causes melting and pore blocking.<sup>49</sup>

**Figure 1.** Particle size distribution (PSD) diagram of OSFA, WFA, and NS samples.

**2.2.3. Chemical Characterization.** The FAs generally showed a high sulfate content which is the primary focus of the selection of these ashes. The main phases in the powdered samples of both FAs included quartz, calcite, and lime. For OSFA, the main sulfate-containing phase is anhydrite while in WFA the main sulfate phase is arcanite. Moreover, free CaO content indicates their potential for  $\text{CO}_2$  sequestration, as CaO is the optimal feedstock for  $\text{CO}_2$  mineral carbonation (Table 3). OSFA exhibited slightly higher free CaO content compared to WFA which is another factor affecting the cementitious properties and  $\text{CO}_2$  uptake. Organic contents of ashes are low as seen from total organic carbon (TOC) values which were calculated based on the values of total carbon (TC) and total inorganic carbon (TIC) (see Table 3). Most of the carbon in the ash belongs to the mineral  $\text{CO}_2$ . OSFA has a much higher  $\text{SiO}_2$  content of 25.21% compared to WFA (3.38%) (Table 3). WFA contained apatite which was not in the OSFA sample. The initial phase composition is not reproduced here as XRD analysis of monoliths is discussed in Section 3.

The presence of quartz in fly ash can provide a surface for the amorphous silica and alumina to nucleate, which can enhance the pozzolanic activity of the fly ash.<sup>52</sup> A higher percentage of  $\text{Al}_2\text{O}_3$  (9.41%) in OSFA can contribute to the formation of ettringite. The NS is mainly containing calcium aluminates with a small amount of  $\text{NbO}_5$  staying in the slag. The unburned carbon content restriction for FA to be used in construction varies based on the intended use and local building codes. However, a common standard for the unburned carbon content in fly ash used in concrete is less than 3%.<sup>53</sup> Typically, WFA has a higher content of heavy metals compared to OSFA. Heavy metals such as Zn, Mn, Cu, and Ba are found in the WFA samples while NS is generally lacking in trace elements (Table 3). OSFA contained Zn, Pb, Ni, Cr, and Ba however in lower concentrations compared to WFA. The effect of carbonation on heavy-metal leaching is discussed in Section 3.2.

**Table 3.** Chemical Composition of OSFA, WFA, and NS (Including TIC, TOC, and Free CaO)<sup>a</sup>

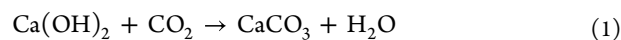
sample	OSFA	WFA	NS
LOI (wt %)	12.85	21.87	—
MgO (wt %)	3.21	5.5	—
$\text{Al}_2\text{O}_3$ (wt %)	9.41	1.01	69.24
$\text{SiO}_2$ (wt %)	25.21	3.38	0.31
$\text{P}_2\text{O}_5$ (wt %)	0.22	5.4	—
$\text{SO}_3$ (wt %)	4.66	7.85	0.08
Cl (wt %)	0.43	0.87	0.1
$\text{K}_2\text{O}$ (wt %)	3.13	7.66	—
CaO (wt %)	36.77	44.89	24.26
$\text{TiO}_2$ (wt %)	0.44	0.08	—
$\text{Fe}_2\text{O}_3$ (wt %)	3.2	0.63	1.19
F (wt %)	0.2	—	—
$\text{NbO}_5$ (wt %)	—	—	4.74
Zn (ppm)	160	2300	—
Sr (ppm)	330	530	370
Rb (ppm)	170	110	—
Pb (ppm)	160	—	—
Ni (ppm)	50	—	160
Mn (ppm)	—	2000	—
Cu (ppm)	—	220	—
Cr (ppm)	100	—	—
Ba (ppm)	480	890	—
TIC (%)	1.25	2.65	—
TC (%)	1.39	3.32	—
TOC (%)	0.14	0.67	—
free CaO (%)	20.37	18.84	—

<sup>a</sup>Note: The “—” symbol represents nonexistent or not applicable data.

### 3. RESULTS AND DISCUSSION

The mechanical, mineralogical, and microstructural features of the monoliths were examined using various techniques such as TGA, XRD, MIP, and SEM-EDS analysis to understand the effects of carbonation and NS addition (Section 3.1). The subsequent analysis focuses on the leaching properties, particularly sulfate leaching, which is the primary emphasis of this paper and is evaluated based on the results of the mineralogical and microstructural analysis (Section 3.2).

**3.1. Effect of Carbonation and NS Addition on Mineralogy and Microstructure.** **3.1.1. General Overview of Strength and  $\text{CO}_2$  Uptake.** In the case of FAs, strength is partially created by the precipitation of carbonate minerals (mainly calcite (eq 1)), which fills the porous structures between the particles and bonds the individual glassy FA particles together.<sup>54</sup> OSFA and WFA monoliths had initial compressive strengths of 11.8 MPa and 9.8 MPa before curing (see Figure 2), respectively. Uibu et al. studied OSA-based concrete development resulting in strength development of up to 14 MPa for CFBC ash after 28 days which shows that the pozzolanic hydration process continues.<sup>55</sup> It is also known that due to the self-cementitious and pozzolanic capabilities of FAs, especially high-calcium FAs with calcium oxide contents higher than 15% in phase composition, an increase in compressive strength can occur as early as 3 days after mixing.<sup>56</sup>



After 4 h carbonation curing it increases almost 4 times to 41.5 MPa for OSFA and 45.1 MPa for WFA monoliths. It should be kept in mind that strength development cannot be solely attributed to calcite formation during carbonation, the



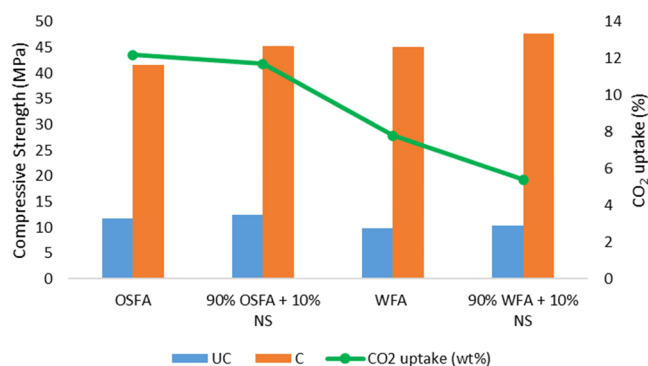


**Figure 2.** Compressive strength results of uncarbonated (UC) and carbonated (C) OSFA, WFA, and NS-added monoliths.

production of hydrated compounds such as CSH continues, contributing to an overall increase in strength. There is an overall higher strength increase in WFA monoliths compared to OSFA monoliths after carbonation despite a lower amount of CO<sub>2</sub> uptake.

NS as an additive further increased the strength to an average of 45.3 MPa for OSFA and 47.7 MPa for WFA. NS addition increases the strength of the UC sample up to 10% before curing and a further increase is followed by carbonation curing. NS introduces calcium aluminates which act as a

supplier of aluminum that reacts during the alkaline activation of aluminosilicate materials, resulting in the creation of binding calcium (aluminate) silicate hydrate (CASH) gels that promote the rapid development of strength.<sup>57–59</sup>

According to the TGA/DTG curves of uncarbonated samples (Figure 3), the main steps in the mass loss process are as follows; the first step is related to water loss from evaporation and later dehydration of crystalline and amorphous components, such as ettringite (AFt) (up to 140 °C)<sup>60,61</sup> and calcium-silicate hydrate (CSH), or calcium aluminate hydrate (CAH), the second is the dehydration of Ca(OH)<sub>2</sub> (410–460 °C), and the third is CO<sub>2</sub> loss from the decomposition of CaCO<sub>3</sub> (600–800 °C). In UC OSFA, a slightly higher peak of ettringite decomposition is observed between 100 and 130 °C compared to C and NS-added samples. Similarly in WFA decomposition around 80 °C was lower in NS-added samples compared to C and UC samples. This finding suggests that CO<sub>2</sub> curing either slowed the formation of AFt, CSH, and CAH or caused their phase change. In both samples, mass loss between 200 and 370 °C can be attributed to CSH decomposition as well as continuing decomposition of monosulfate after ettringite decomposes.<sup>60,62</sup> In carbonated OSFA samples, the NS-added sample shows higher mass loss due to the decomposition of Ca(OH)<sub>2</sub> and lower mass loss in the decomposition of CaCO<sub>3</sub> compared to the carbonated sample which indicates a slight negative effect

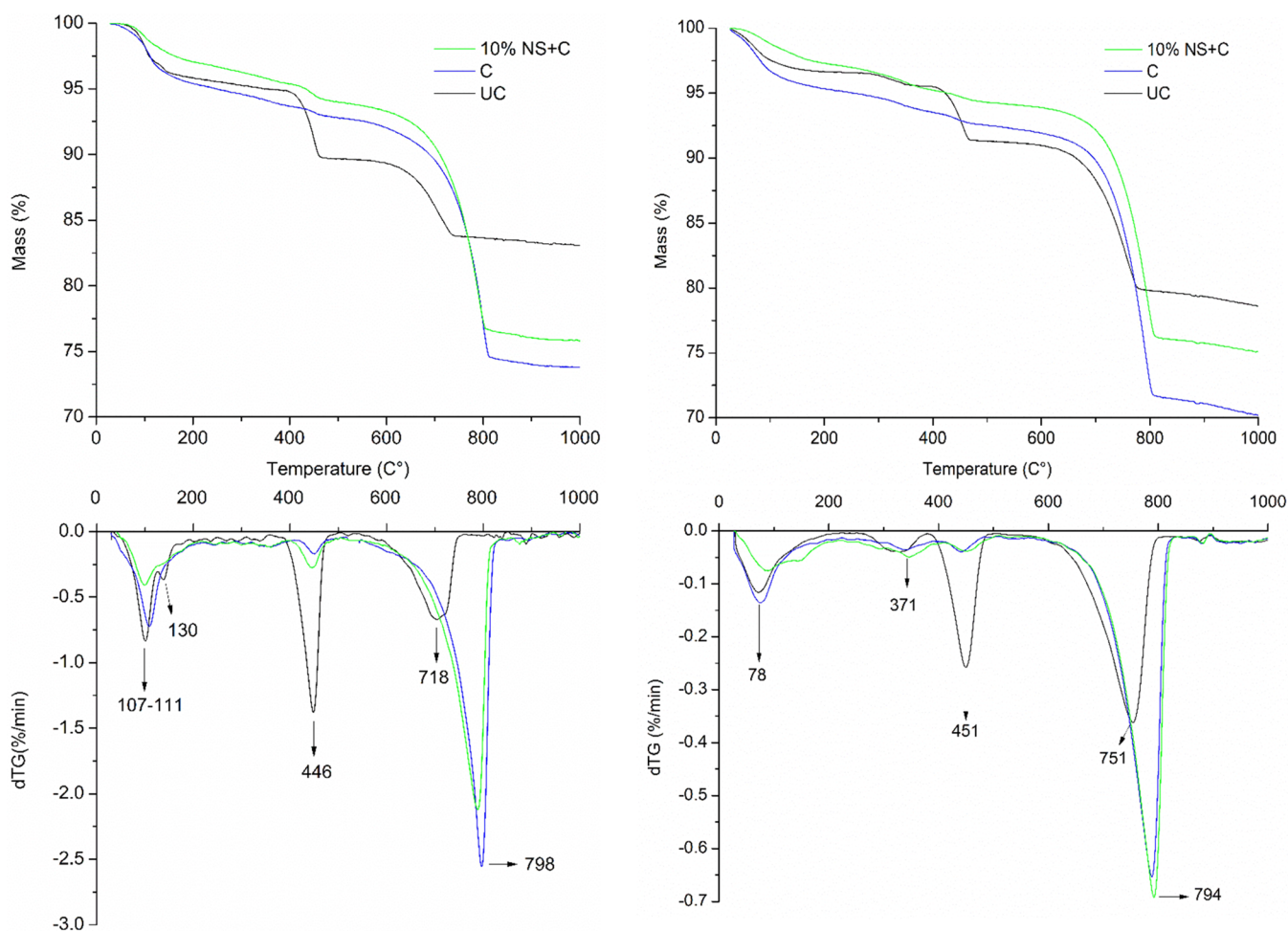


**Figure 3.** TGA and DTG patterns of OSFA (left) and WFA (right) compacts that are uncarbonated (UC), carbonated (C), and niobium slag-added (10% NS + C).

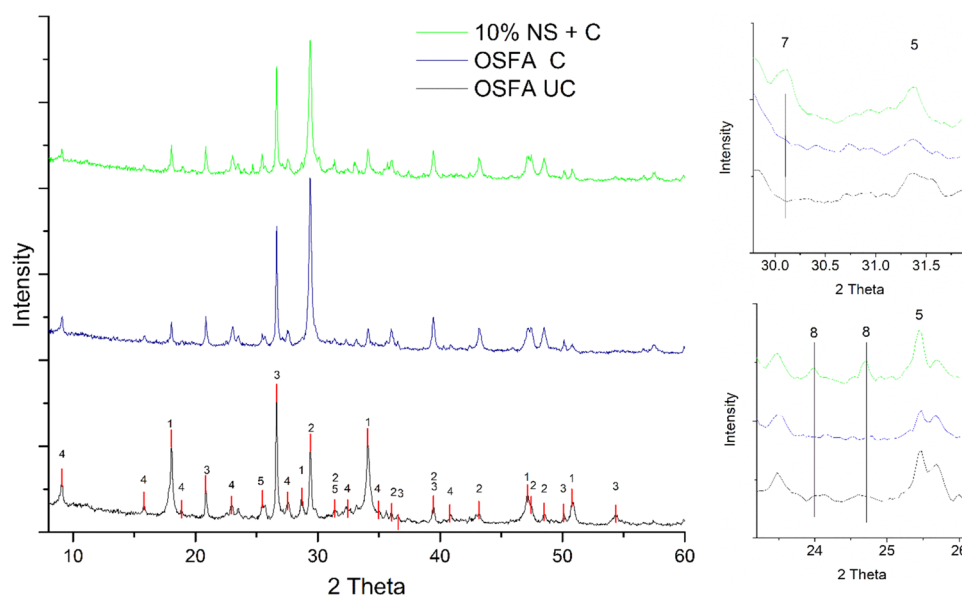


**Figure 4.** XRD patterns of OSFA samples (1—portlandite, 2—calcite, 3—quartz, 4—ettringite, 5—anhydrite, 7—CAH, 8—CAS).

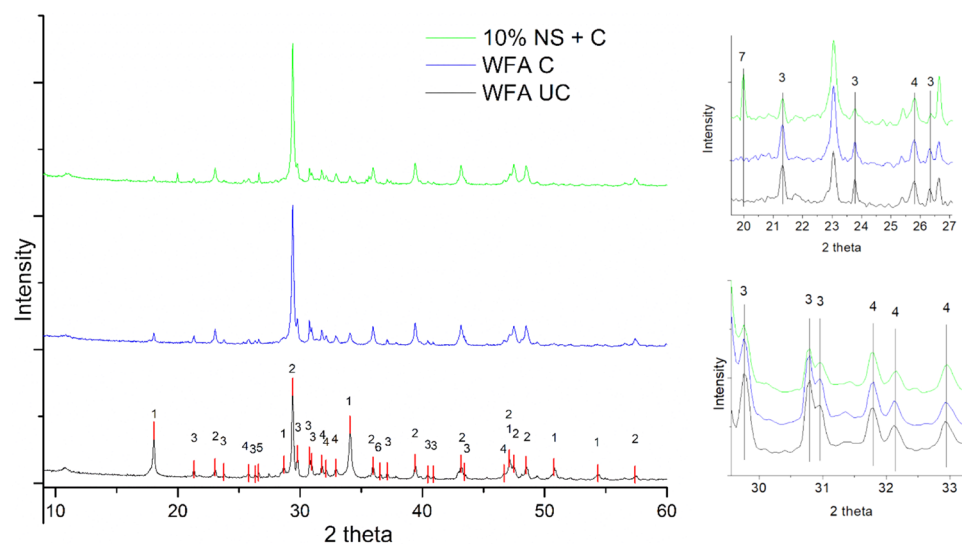


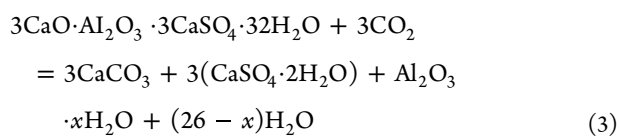
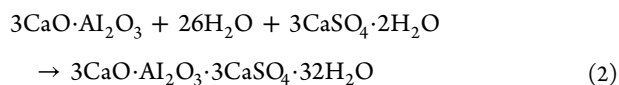
**Figure 5.** XRD patterns of WFA samples (1—portlandite, 2—calcite, 3—arcanite, 4—hydroxyapatite, 5—quartz, 6—periclase, 7—CAH).

of NS on carbonation. The initial (uncarbonated) mineral  $\text{CO}_2$ -associated mass loss is taken into consideration to determine the net  $\text{CO}_2$  absorption. The net  $\text{CO}_2$  uptake of the 100% OSFA sample is 12.2% and NS-added OSFA sample is 11.7%. 100% WFA sample and NS-added WFA samples are 7.8 and 5.4%, respectively. Lower  $\text{CO}_2$  uptake of NS-added samples can be explained by the fast hydration of calcium aluminates changing pore structures causing less available surface area and a lower percentage of portlandite, which is the main phase contributing to carbonation, due to the replacement of ash with NS.

**3.1.2. Mineralogical Characterization.** **3.1.2.1. XRD Analysis.** XRD analysis of monoliths made of OSFA and WFA together with NS-added monoliths is performed to see the changes in the phases after carbonation and NS addition. The main constituents in OSFA UC monoliths include portlandite, calcite, and quartz, while smaller peaks of ettringite, anhydrite, orthoclase, and hematite were identified (Figures 4 and 5). The main changes identified after the carbonation of OSFA

monoliths included the intensity of portlandite as well as anhydrite peaks which are less intense in carbonated monoliths while showing higher intensity in NS-added monoliths. Ettringite formation (eq 2) occurs during the hydration period of samples which is supported by the XRD pattern as well as the TGA of the UC OSFA samples. It is created when calcium and alumina, both of which are present in cementitious matrices and supplementary cementitious materials (in this case NS), react with sulfate, which is either naturally present in the cement paste or is introduced into the system from an outside source<sup>63–65</sup> Delayed formation of ettringite can be harmful to ordinary cement systems; however, in calcium aluminate cement systems, ettringite formed during hydration is typically the most significant hydrate and is substantially in charge of these systems' unique characteristics, including quick setting, quick hardening, quick drying, and compensating for shrinkage.<sup>66</sup> Decomposition of ettringite is observed after carbonation which can form in addition to calcium carbonate, gypsum, and alumina gel.<sup>67</sup> In comparison to anhydrite and

ettringite, gypsum is more soluble, releasing more sulfates into the carbonated OSFA monolith's leachate.



In NS-added monoliths, calcium aluminate hydrate peaks as well as partial conversion of ettringite to amorphous phases are observed. The partial reduction of ettringite can also be observed in TGA patterns (Figure 3). The main sulfate-bearing phases are, namely, arcanite for WFA and anhydrite for OSFA. Ettringite formation in WFA monoliths during the hydration period is observed to be lower compared to OSFA. This can be explained by the lower Al content in WFA and the different behavior of sulfate-bearing phases (arcanite and anhydrite) in both ashes. In NS-added monoliths of WFA, the intensity of arcanite peaks is lower compared to UC and C monoliths which could indicate the binding of sulfates in amorphous calcium aluminate phases observed by SEM-EDS analysis (Figures 8 and 9). Hydroxyapatite which is also (Figure 5) observed in WFA monoliths can be partially responsible for high compressive strength values (Figure 2).<sup>68</sup> Changes in the CAS phases are discussed in Section 3.2 and explained in greater detail with the aid of additional figures, in conjunction with the sulfate leaching process. However, it can be difficult to determine the exact phases due to the amorphous nature and complex structure of the material.

**3.1.3. Microstructural Characterization. 3.1.3.1. MIP Analysis.** Pore structure and porosity are additional crucial elements that identify the physical strength of solidified structures. To investigate the impact of carbonation on the microstructure of the hardened monoliths, mercury intrusion porosimetry (MIP) was used to estimate the pore size distribution of the OSFA and WFA monoliths. A nonwetting liquid (one with a contact angle larger than 90°) will only infiltrate capillaries under pressure, according to the theory underlying MIP. Washburn as cited by Diamond<sup>69</sup> explains the relationship between pressure and capillary diameter (eq 4)

$$P = \frac{4\gamma \cos \theta}{d} \quad (4)$$

where  $P$  is the pressure,  $\gamma$  is the surface tension of the liquid,  $\theta$  is the contact angle of the liquid (140° is selected), and  $d$  is the diameter of the capillary. The volume intruded at each pressure increment is used to calculate the pore size distribution. The entire volume of intruded pores is used to calculate total porosity. It should be noted that the MIP technique measures pore entrance size rather than pore size,<sup>70</sup> only the open porosity is determined using the MIP technique currently in use. The "ink-bottle effect" is a phenomenon that causes big pores to be underestimated and small pores to be overestimated.<sup>71</sup> The degree to which hydrated cementitious materials are porous depends mainly on the fineness of the particles, the water-to-solid ratio, the method of mixing, and the curing circumstances.

The MIP analysis revealed that OSFA monoliths exhibit a decline in macropores upon carbonation,<sup>72</sup> causing the associated compressive strength to rise from 11.8 to 41.5

MPa (Figures 6 and 7). Total porosity diminishes with increasing calcite deposition as well as the filling effect of

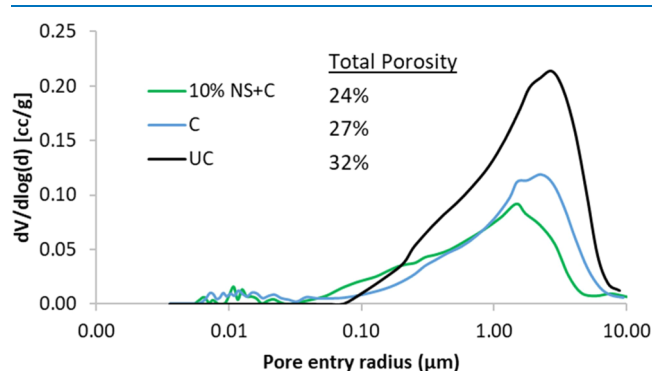


Figure 6. OSFA pore size distribution with total porosity values.

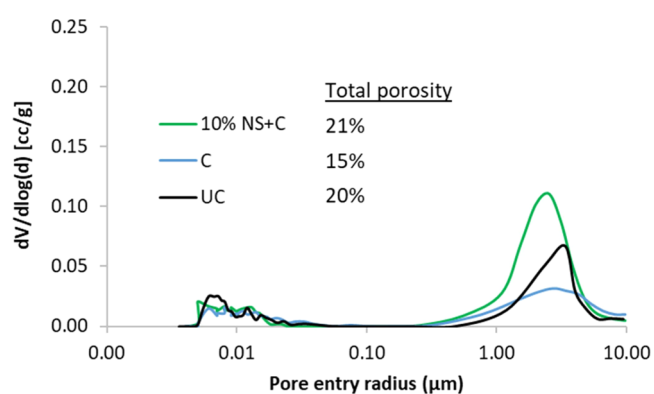
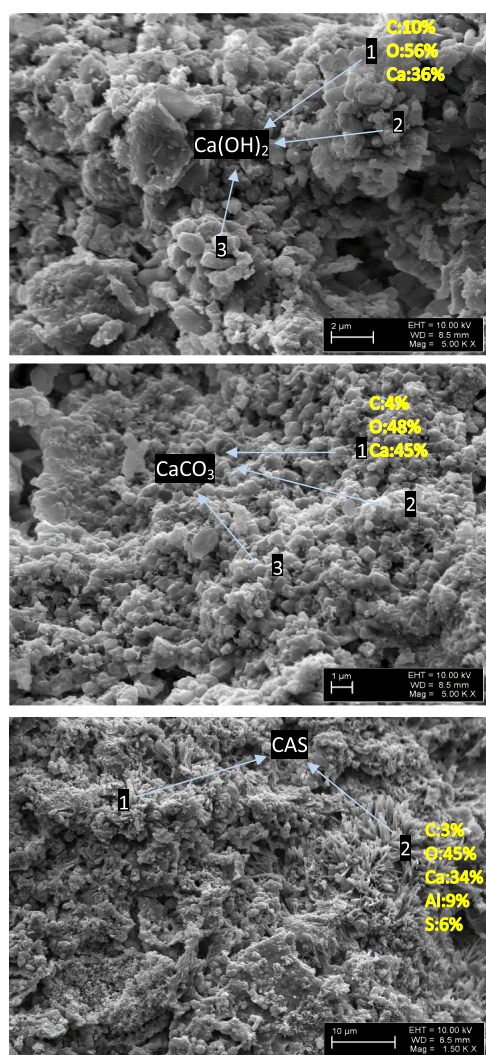


Figure 7. WFA pore size distribution with total porosity values.

hydrated phases, and the decline becomes more significant. Calcite is deposited on the inside of pores as well as at their entry during carbonation, obstructing some of these pores and blocking mercury infiltration. NS-added carbonated monoliths showed slightly lower macropores compared to carbonated OSFA monoliths. Upon carbonation, a partial decrease in ettringite can cause an overall increase in porosity due to its high molecular volume and low density. In the case of OSFA, this effect is mitigated by the subsequent formation of calcite polymorphs. In the case of WFA, the carbonation effect is also clear in the reduction of macropores. However, NS-added WFA monoliths showed higher macropores compared to 100% WFA monoliths which can be explained by the particle size difference between NS which has much coarser particles, and WFA, affecting pore mouth formations during hydration. The reason for the lower total porosity values in monoliths made from WFA compared to OSFA may be attributed to the different compaction properties of the ashes, which results in a denser structure upon compaction for WFA.

**3.1.3.2. SEM-EDS Analysis.** The morphological changes and chemical composition were identified by SEM images (1000–5000 times magnified) and EDS analysis of UC, C, and NS-added monoliths, which are reproduced in greater detail and attached as the Supporting Information to this publication. An image of the OSFA UC monolith with hexagonal lamellar portlandite crystals can be seen in Figure 8. The particles have a gritty appearance with some stubby laths and noticeable big pores. The EDS of UC monoliths reveals that the products are an amalgam of calcium and oxygen, validating the elemental





**Figure 8.** SEM images and numbered positions for quantitative EDS analysis of OSFA uncarbonated (top), carbonated (middle), and niobium slag-added (bottom).

ratio for  $\text{Ca}(\text{OH})_2$  crystals. In the WFA UC image, spherical glassy FA particles surrounded by hydrated products can be clearly identified. In OSFA C monolith Polymorphs of calcium carbonate precipitated on carbonation in acicular and globular formation intermixed with decalcified C–S–H or silica gel. While carbonated WFA monoliths have shown Calcite formations like OSFA monoliths, smoother gel-like surfaces were more abundant with less porous structure (Figure 9) in WFA monoliths. EDS has shown, some of these areas include a mix of many elements in combined amorphous matrixes.

NS-added monoliths have exhibited needle-like CAS crystal growths in addition to calcite polymorphs (Figures 8 and 9). WFA monoliths were observed to be much denser in general and less porous compared to OSFA monoliths which are in line with MIP analysis results (Figures 6 and 7). SEM investigations along the sample depth of the carbonated monoliths have revealed that clusters of portlandite crystals are present only in the deeper part of the monolith. There are two tenable explanations for this imperfect conversion that work in tandem. The first is that the initial carbonated layer provides a macroscopic layer that inhibits the  $\text{CO}_2$  gas diffusion to the portlandite crystals. Due to the pore closure brought on by the

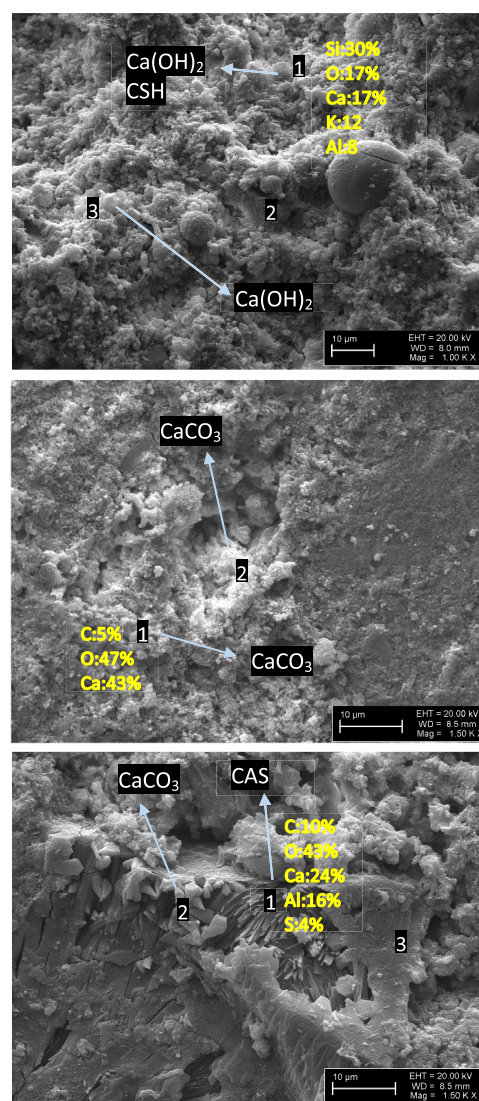


**Figure 9.** SEM images and numbered positions for quantitative EDS analysis of WFA uncarbonated (top), carbonated (middle), and niobium slag-added (bottom).

precipitation of bigger  $\text{CaCO}_3$  crystals ( $36.9 \text{ cm}^3/\text{mol}$ ) than  $\text{Ca}(\text{OH})_2$  crystals ( $33.6 \text{ cm}^3/\text{mol}$ ) on the pore throats, it is anticipated that this carbonated layer will be less permeable.<sup>73,74</sup> The second reason can be due to the enhanced carbonation reaction's exothermic nature and the reduced hydrophilicity of  $\text{CaCO}_3$  crystals compared to  $\text{Ca}(\text{OH})_2$  crystals, there is not enough water present for the reaction to take place.<sup>75</sup>

### 3.2. Effect of Carbonation and Niobium Slag Addition to Leaching Properties. 3.2.1. Sulfate Leaching.

The release of hazardous substances into the environment is one of the most crucial factors for waste disposal in landfills or reuse. The Criteria and Procedures for The Acceptance of Waste at Landfills established in the Council Directive 1999/31/EC of 26 April 1999<sup>76</sup> gives criteria for waste landfills, in which the wastes sent to landfill are classified into three categories, “inert,” “nonhazardous” and “hazardous” in terms of their leachability and stability. For sulfates, leaching limits for these landfills are 1000, 20 000, and 50 000 mg/kg of waste, respectively.

As  $\text{Ca}(\text{OH})_2$  becomes depleted in the monoliths of OSFA, pH steadily declines from around 12.8 at the initial stage to around 11.4 as demonstrated by the pH measurements of the subsequent leachates (Figure 10). For WFA, a similar decrease

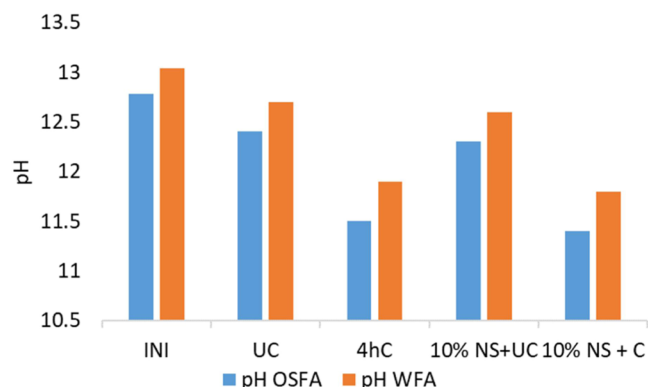


**Figure 10.** pH values of OSFA and WFA monoliths together with initial ash samples (INI).

in pH levels from an initial 13.1 to around 11.8 is observed. pH levels for OSFA and WFA UC monoliths are in the range of 12.3–12.7 which decreases after carbonation to the range of 11.4–11.9. It is noted that after NS addition pH still decreases compared to UC NS-added monolith, which supports that the carbonation reaction is not fully hindered. The stability domain for sulfate ettringite commonly lies between 10.5 and 13 at the various pH ranges described in the literature.<sup>77,78</sup>

Sulfate leaching tests revealed that for 100% OSFA sulfate concentration is increased from 2260 mg/kg to 6510 mg/kg after carbonation (Figure 11). However, 10% NS-added OSFA monoliths showed no detectable sulfate leaching for both uncarbonated and carbonated monoliths. Increased leaching of sulfates in carbonated OSFA monoliths was seen compared to uncarbonated ones due to the carbonation of ettringite. The addition of 10% NS reduced the leaching of sulfate to an undetectable range (less than 2 mg  $\text{SO}_4^{2-}$ /kg of ash) and it stayed in that range after carbonation as well, which shows the addition of NS is successful at curbing the negative effect of carbonation in sulfate leaching for OSFA monoliths. WFA exhibited much higher sulfate leaching levels compared to OSFA, which can be due to already higher initial concentration in WFA and higher solubility of arcanite compared to anhydrite.<sup>79</sup> Ettringite and other CAS formation in WFA monoliths during the hydration period is observed to be much

lower compared to OSFA monoliths. In contrast to OSFA, WFA did not display an increase in leached sulfate upon carbonation which can be explained by the lack of ettringite formation which is the main cause of the increase in sulfate leaching in OSFA. Yet, in WFA monoliths slight decrease after carbonation is observed, which can be due to the physical encapsulation of sulfates with the formation of calcite. In WFA, NS addition significantly lowers sulfate leaching concentration before carbonation and a further decline is observed after carbonation. The decline of around 14 000 mg  $\text{SO}_4^{2-}$ /kg of ash with the addition of NS and carbonation compared to 100% WFA concentration is also considerably high in WFA.

The rapid hydration of calcium aluminates can provide an initial source of calcium ions, which can promote the carbonation of FA by providing a surface for the carbon dioxide to react. This can potentially enhance the carbonation potential of FAs and increase the sequestration of carbon dioxide in the cementitious system.<sup>57</sup> Additionally, it is important to note that the rapid hydration of calcium aluminates can also lead to the formation of CAS phases, which can consume sulfate ions and reduce the availability of these ions for sulfate mobility.

SEM images of NS-added monoliths together with mineralogical analysis are examined in connection with sulfate leaching. When niobium slag is added, the system's mineralogical state changes along with the chemistry of the hydrated phases, which can have a significant impact on the bound sulfate (Figures 12 and 13). In general, it can be deduced that both carbonation and NS addition have effects on the mobility of sulfates in OSFA and WFA which can be associated with chemical and physical changes in the monolith microstructure. This mechanism involves complex interrelated microstructural, mechanical, and CSH chemistry considerations.<sup>80,81</sup> According to clinker mineralogy, the hydrated phases include AFt, AFm, and CSH. Ettringite crystals fix  $\text{SO}_4$ , while AFm and CSH phases also help fix heavy metals in the matrix.<sup>82,83</sup> Figure 11 shows a SEM image of the NS-added OSFA monolith with sections of the XRD pattern including known peaks of CAS. Peaks of ettringite are still stable after carbonation however less in NS-added monoliths. Also, other peaks of different phase structures of CAS become more visible with NS addition. For OSFA, it can be deduced that different phases of CAS are seen along with anhydrite becoming more stable in the NS-added monoliths. According to Xu et al., the presence of anhydrite increases the stability of ettringite compared to other sources of calcium sulfate.<sup>84</sup> For WFA, a similar SEM image of NS-added monolith shows the clearer

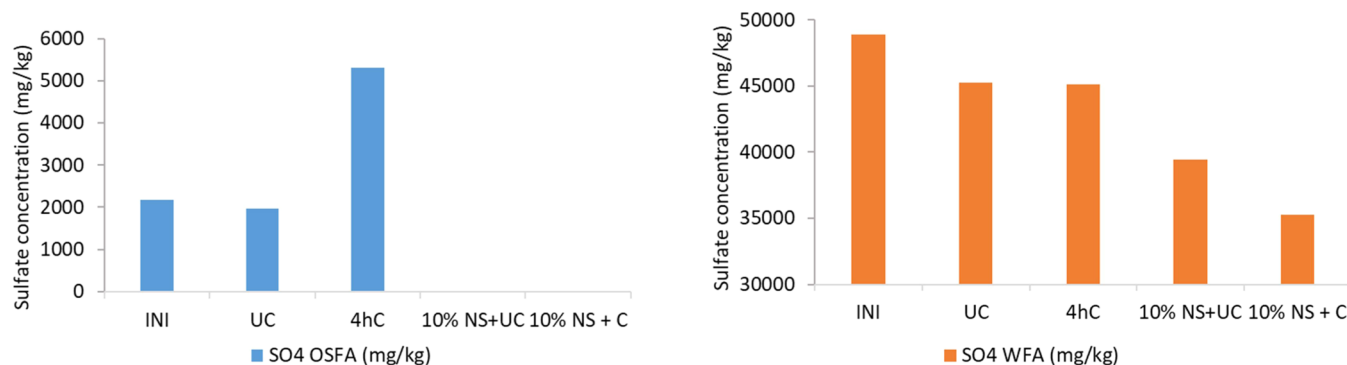


**Figure 11.**  $\text{SO}_4^{2-}$  Leaching values of OSFA (left) and WFA (right) monoliths together with initial ash samples (INI).



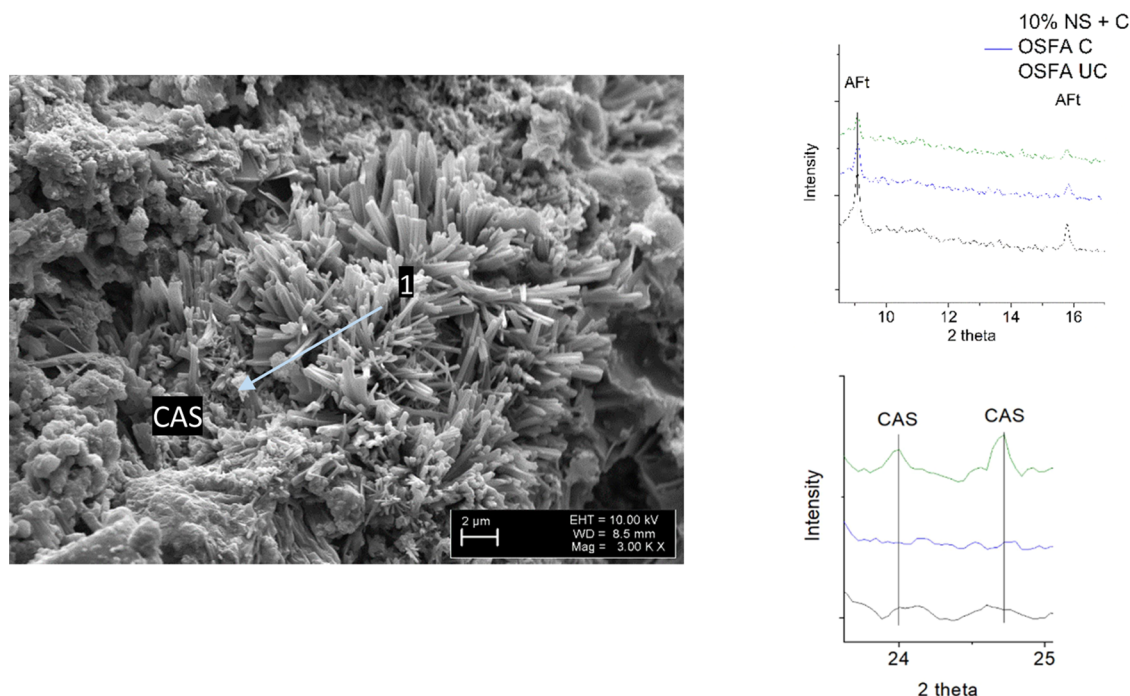


Figure 12. SEM image of NS-added OSFA with sections of XRD pattern detailing CAS peaks.

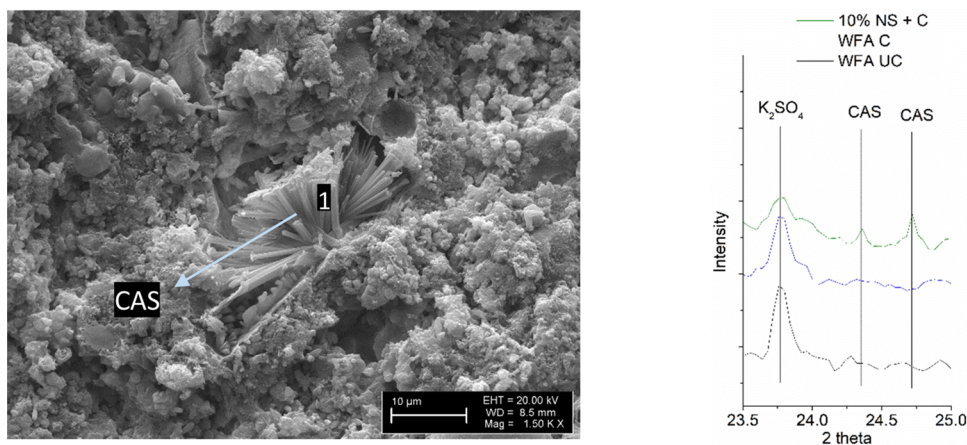


Figure 13. SEM image of NS-added WFA with sections of XRD pattern detailing  $K_2SO_4$  and CAS peaks.

structure of needle-like formation, with sections of XRD pattern including arcanite and CAS phases. In WFA monoliths, sulfate-bearing arcanite seemed to be in less intensity and CAS phases are more distinguishable in the case of NS addition.

According to the mineralogical analysis, the highly soluble minerals halite and sylvite contain chloride ions. As a result, as indicated in Figure 14, the chloride release values from monoliths are lower than the landfill limits for nonhazardous wastes. Carbonation has slightly decreased  $Cl^-$  leaching concentrations for both OSFA and WFA monoliths. NS addition has decreased the mobility of  $Cl^-$  greatly for WFA and a further decrease occurred after the carbonation of NS-added monoliths. It can be said that both  $SO_4^{2-}$  and  $Cl^-$  mobility in WFA monoliths exhibited a similar trend after the NS addition and carbonation process. For OSFA  $Cl^-$  leaching values were not greatly affected by the NS addition or carbonation process. All  $Cl^-$  leaching levels are under the landfill limit for nonhazardous wastes which is 15 000 mg/kg of waste.

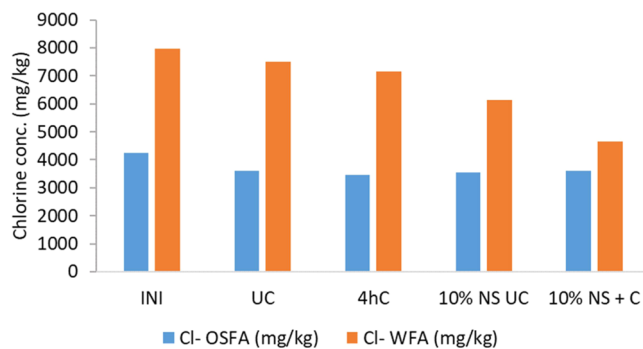


Figure 14.  $Cl^-$  leaching values of OSFA and WFA monoliths together with initial sample (INI).

Leaching results indicate that after carbonation curing, for OSFA the levels of Cr, Cu, and Zn, and for WFA the level of Ba slightly increased (Table 4). However, all of the heavy-metal leaching values were reduced with the addition of NS.



Table 4. Leaching Levels of Trace Elements in OSFA and WFA Ash and Monoliths with Landfill Limits (ppm)<sup>a</sup>

	OSFA				WFA				inert	nonhazardous
	INI	UC	C	10% NS + C	INI	UC	C	10% NS + C		
Ba	5.4	4.5	4.1	5.1	1.4	1	1.3	0.4	20	100
Cd	tr	tr	tr	tr	tr	tr	tr	tr	0.04	1
Cr	1	1.4	2	0	5.2	5.2	4.5	3.4	0.5	10
Cu	2.9	1	1.5	0.4	2.2	1.2	1	1	2	50
Mn	tr	tr	tr	tr	tr	tr	tr	tr	na	na
Ni	tr	tr	tr	tr	tr	tr	tr	tr	0.4	10
Pb	tr	tr	tr	tr	tr	tr	tr	tr	0.5	10
Rb	11.2	10.7	3.3	3	321.8	301.2	257.2	145.8	na	na
Sr	157.6	108.1	46.7	31.8	33.9	27.3	12.8	4.2	na	na
Zn	5.8	0.5	3.8	tr	4.7	tr	tr	tr	4	50

<sup>a</sup>tr = trace amount, na = not applicable.

For heavy metals, all of the leaching values are under the limit for landfills for nonhazardous waste. For OSFA, the limit values also for landfilling inert waste were not breached except for Cr, Cu, and Zn which were all under the limit in the NS-added monoliths. For WFA monoliths Cr was the only element that stayed above the inert landfill limit, while Zn and Cu were under the limit for uncarbonated samples. Mobility of Sr and Rb was greatly reduced after carbonation and NS addition for both WFA and OSFA monoliths. Irha et al.<sup>85</sup> and Uibu et al.<sup>55</sup> have addressed the leaching behaviors of various types of OSFA as well as OSFA-based mortars. Although the leachates under study were highly alkaline and saturated with various ions (the predominant ions were Ca<sup>2+</sup>, K<sup>+</sup>, Na<sup>+</sup>, and SO<sub>4</sub><sup>2-</sup>), their research shows that during the curing process, the fraction of readily soluble inorganic components reduced while the mobility of potentially hazardous Cd and Zn did not change. EC values exhibit a decrease with carbonation due to the carbonated layer reducing the availability of free ions in the material, which are responsible for conducting electricity (Figure 15). The formation of the carbonated layer also

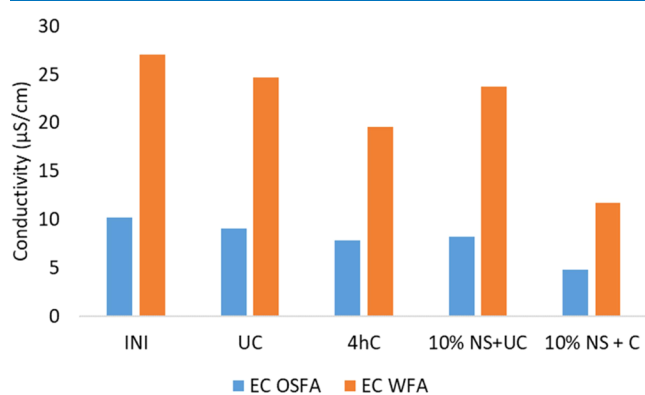


Figure 15. EC values of OSFA and WFA monoliths together with initial sample (INI).

reduces the porosity of the material, which can further limit the movement of ions and contribute to the reduction in EC. As a result of changes in the chemical composition and physical characteristics of the FA monoliths brought on by carbonation and the addition of NS, ions as well as heavy metals get immobilized, limiting the availability of these for EC.

#### 4. DISCUSSION

Worldwide, there is a growing trend among industries to produce and apply cement-free or low-carbon building materials that are strengthened through carbonation. Despite the growing interest in the use of FA as an SCM or in general construction applications, the utilization of HSFAs remains largely unexplored.<sup>86</sup> CO<sub>2</sub> mineralization processes could benefit from using alternative HSFAs streams, particularly those not meeting the relevant standards (as per ASTM C618), as raw materials.<sup>87</sup>

A comparative analysis of CO<sub>2</sub> uptake across various studies reveals a broad spectrum of results, primarily contingent upon the specific material under investigation. For instance, Srivastava et al. reported CO<sub>2</sub> uptake values of ~18 to 21% for Basic Oxygen Furnace slags after a reaction time of 4 h.<sup>88</sup> Conversely, electric arc furnace slag exhibited a more gradual increase in CO<sub>2</sub> uptake, ranging from 7 to 12% over the same duration. While Mo et al. reported that steel slag pastes carbonated at 0.1 MPa CO<sub>2</sub> for 24 h reached levels of CO<sub>2</sub> uptake between 11 and 17%.<sup>89</sup>

In the case of fly ash, Li et al. reported a substantial variation in CO<sub>2</sub> uptake, ranging from 6 to 21%, which was attributed to the different CaO contents in the Coal Fly Ash.<sup>90</sup> Class C Fly Ash, with a CaO content of 15–50%, carbonates rapidly and possesses sufficient strength for structural construction, thereby presenting a higher potential for CO<sub>2</sub> sequestration than Class F Fly Ash, which contains 1.5–5% CaO.<sup>91,92</sup> Zhang et al. developed an eco-cement from municipal solid waste residue and Ca(OH)<sub>2</sub>, which demonstrated a CO<sub>2</sub> uptake of around 8%.<sup>93</sup> In a separate study, cement kiln dust, characterized by its high CaO content (20–60%), demonstrated a CO<sub>2</sub> uptake ranging from 4 to 8%.<sup>94</sup> The CO<sub>2</sub> sequestration potential of industrial solid wastes depends on their alkalinity content and various operating parameters associated with the carbonation process, as well as the waste production process affecting its physical and chemical characteristics.

In this context, the CO<sub>2</sub> uptake capacities achieved in this study are noteworthy. Specifically, the capacities range from 11.7 to 12.2% for OSFA and from 5.4 to 7.8% for WFA. These figures are not only comparable to those reported in other studies but are also crucial because the addition of niobium slag (NS) did not significantly hinder the carbonation potential of the residues, while it mitigated sulfate leaching. These findings highlight the feasibility of repurposing underutilized wastes such as HSFAs to produce construction materials

through accelerated carbonation. This approach aligns with broader goals of waste management and carbon sequestration, further emphasizing the importance of this study.

## 5. CONCLUSIONS

This study analyzes the environmental and microstructural properties of carbonate-bonded monoliths composed of HSFA and niobium slag NS enriched with calcium aluminate. A significant finding of our research is the considerable increase in the initial compressive strength of the monoliths post-carbonation (up to 41.5 MPa for OSFA and 45.1 MPa for WFA), which underlines the potential of this method for enhancing the structural integrity of HSFA-based construction materials. In addition, our findings reveal that the inclusion of NS leads to a further increase in strength without substantially impacting CO<sub>2</sub> uptake. This is a noteworthy discovery as it suggests that NS can be employed to bolster the mechanical properties of HSFA-based materials without impeding their carbon sequestration potential. Another key finding of our study is the general decline in leaching values, particularly sulfates and heavy metals, upon the introduction of NS. This suggests that the addition of NS can effectively immobilize harmful substances in HSFA. The experimental results of this study can be summarized as follows.

- The pH change is not solely dependent on the consumption of portlandite since carbonation curing slightly decreased the leachate pH due to the prolonged hydration reactions as well as the chemical and mineralogical composition of different FAs.
- MIP showed a decrease in macropores in carbonated and NS-added OSFA monoliths. In WFA monoliths the overall porosity was lower compared to OSFA, while NS addition did not decrease macropores due to particle size difference.
- For NS-added OSFA and WFA monoliths, all of the heavy-metal levels are reduced with the ion-stabilizing effect of hydrated calcium aluminate silicate gel.
- Anhydrite-bearing OSFA monoliths showed increased formation of ettringite compared to arcanite-bearing WFA monoliths.
- In NS-added monoliths, anhydrite, arcanite, ettringite, and different CAS phases are identified as main sulfate-bearing phases through SEM-EDS and XRD analyses.

Based on these findings, it can be concluded that the leaching of sulfates is effectively mitigated through a dual mechanism involving both the chemical binding to calcium aluminate silicate (CAS) phases and the physical entrapment within the structure of calcium aluminate silicate hydrate (CA(S)H) gels.

This research effectively showcases the potential of upcycling HSFAs through the outlined carbonation method incorporating calcium aluminate-rich NS. This process not only presents an opportunity to utilize these waste materials in the construction industry but also demonstrates significant sulfate immobilization as a key finding.

## ■ ASSOCIATED CONTENT

### SI Supporting Information

The Supporting Information is available free of charge at <https://pubs.acs.org/doi/10.1021/acsomega.3c03286>.

Quantitative EDS analysis tables corresponding to Figures 8 and 9 (PDF)

## ■ AUTHOR INFORMATION

### Corresponding Author

Mustafa Cem Usta – Department of Materials and Environmental Technology, Tallinn University of Technology, 19086 Tallinn, Estonia; [orcid.org/0000-0003-3021-2656](https://orcid.org/0000-0003-3021-2656); Email: [mustafa.usta@taltech.ee](mailto:mustafa.usta@taltech.ee)

### Authors

Can Rüstü Yörük – Department of Materials and Environmental Technology, Tallinn University of Technology, 19086 Tallinn, Estonia

Mai Uibu – Department of Materials and Environmental Technology, Tallinn University of Technology, 19086 Tallinn, Estonia

Reiner Traksmaa – Department of Mechanical and Industrial Engineering, Tallinn University of Technology, 19086 Tallinn, Estonia

Tiina Hain – Department of Civil Engineering and Architecture, Tallinn University of Technology, 19086 Tallinn, Estonia

Andre Gregor – Department of Materials and Environmental Technology, Tallinn University of Technology, 19086 Tallinn, Estonia

Andres Triikkel – Department of Materials and Environmental Technology, Tallinn University of Technology, 19086 Tallinn, Estonia

Complete contact information is available at:

<https://pubs.acs.org/10.1021/acsomega.3c03286>

### Notes

The authors declare no competing financial interest.

## ■ ACKNOWLEDGMENTS

This work was carried out as part of a Ph.D. project supported by the Estonian Ministry of Education and Research (IUT33-19). This work was partially supported by ASTRA “TUT Institutional Development Program for 2016–2022” Graduate School of Functional Materials and Technologies. The help of Mart Viljus (SEM images) and Oliver Jarvik is gratefully acknowledged.

## ■ REFERENCES

- (1) ASTM C618: *Standard Specification for Coal Fly Ash and Raw or Calcined Natural Pozzolan for Use in Concrete* ASTM International: West Conshohocken, PA; 2022.
- (2) EN 450-1: *Fly Ash for Concrete – Definition, Specifications, and Conformity Criteria* British Standards Institution: London, U.K.; 2012.
- (3) JIS R 5213: *Portland Fly-Ash Cement (Amendment 1)* Japanese Standards Association: Tokyo, Japan; 2009.
- (4) Usta, M. C.; Yörük, C. R.; Hain, T.; Paaver, P.; Snellings, R.; Rozov, E.; Uibu, M.; et al. Evaluation of New Applications of Oil Shale Ashes in Building Materials. *Minerals* **2020**, *10*, 765.
- (5) Usta, M. C.; Yörük, C. R.; Uibu, M.; Hain, T.; Gregor, A.; Triikkel, A. CO<sub>2</sub> Curing of Ca-Rich Fly Ashes to Produce Cement-Free Building Materials. *Minerals* **2022**, *12*, 513.
- (6) Socié, A.; Dubois, F.; Monerie, Y.; Neji, M.; Perales, F. Simulation of Internal and External Sulfate Attacks of Concrete with a Generic Reactive Transport-poromechanical Model. *Eur. J. Environ. Civ. Eng.* **2022**, 1–28.
- (7) Neto, J. S. A.; Angeles, G.; Kirchheim, A. P. Effects of Sulfates on the Hydration of Portland Cement—A Review. *Constr. Build. Mater.* **2021**, *279*, No. 122428.
- (8) Kaladharan, G.; Rajabipour, F. Evaluation and Beneficiation of High Sulfur and High Alkali Fly Ashes for Use as Supplementary

- Cementitious Materials in Concrete. *Constr. Build. Mater.* **2022**, *339*, No. 127672.
- (9) Papadakis, V. G.; Tsimas, S. Supplementary Cementing Materials in Concrete: Part I: Efficiency and Design. *Cem. Concr. Res.* **2002**, *32*, 1525–1532.
- (10) Hou, P. K.; Qian, J. S.; Wang, Z.; Deng, C. Production of Quasi-sulfoaluminate Cementitious Materials with Electrolytic Manganese Residue. *Cem. Concr. Compos.* **2012**, *34*, 248–254.
- (11) Zhang, Y.; Wang, J.; Zhang, L.; Li, C.; Jiang, H.; Ba, X.; Hou, D. Study on the Preparation and Properties of High-belite Cementitious Materials from Shield Slag and Calcium Carbide Slag. *Constr. Build. Mater.* **2022**, *355*, No. 129082.
- (12) European Union. Regulation (EU) No 305/2011 of the European Parliament and of the Council of 9 March 2011. Laying Down Harmonised Conditions for the Marketing of Construction Products and Repealing Council Directive 89/106/EEC, 2011. <http://data.europa.eu/eli/reg/2011/305/oj>.
- (13) Ragipani, R.; Escobar, E.; Prentice, D.; Bustillos, S.; Simonetti, D.; Sant, G.; Wang, B. Selective sulfur removal from semi-dry flue gas desulfurization coal fly ash for concrete and carbon dioxide capture applications. *Waste Manage.* **2021**, *121*, 117–126.
- (14) Wang, W.; Luo, Z.; Shi, Z.; Cen, K. Thermodynamic analysis of ash mineral phases in combustion of high-sulfur coal with lime. *Ind. Eng. Chem. Res.* **2011**, *50*, 3064–3070.
- (15) Duc, N. V. Experimental Water Quality Analysis from the Use of High Sulfuric Fly Ash as Base Course Material for Road Building. *Eng. Technol. Appl. Sci. Res.* **2019**, *9*, 4627–4630.
- (16) Shin, J. H.; Park, J. H. Formation mechanism of oxide-sulfide complex inclusions in high-sulfur-containing steel melts. *Metall. Mater. Trans. B* **2018**, *49*, 311–324.
- (17) Singh, A. K.; Chandra, R. Pollutants released from the pulp paper industry: Aquatic toxicity and their health hazards. *Aquat. Toxicol.* **2019**, *211*, 202–216.
- (18) Luong, L. D.; Nguyen, D. V.; Luu, H. T.; Le, H. V.; Nguyen, T. M. Study on fluidized bed combustion fly ash with high sulfur from Cao Ngan coal-fired thermal power plant for production of construction materials. *Vietnamese J. Sci. Technol.* **2010**, *1–2*, 8–16.
- (19) Shon, C. S.; Saylak, D.; Mishra, S. In *Evaluation of Manufactured Fluidized Bed Combustion Ash Aggregate as Road Base Course Material*, World of Coal Ash Conference, Denver, USA, May 9–12, 2011.
- (20) Gazdič, D.; Fridrichova, M.; Kulisek, K.; Vehovska, L. The potential use of the FBC ash for the preparation of blended cements. *Procedia Eng.* **2017**, *180*, 1298–1305.
- (21) Xie, X. M.; Guo, L. In *Study on Preparation and Properties of Fly Ash Concrete with High Sulfur and High-Calcium Fly*, 2nd IEEE International Conference on Information Management Engineering, Chengdu, China, April 16–18, 2010.
- (22) Bogush, A. A.; Stegemann, J. A.; Roy, A. Changes in composition and lead speciation due to water washing of air pollution control residue from municipal waste incineration. *J. Hazard. Mater.* **2019**, *361*, 187–199.
- (23) Yang, Z.; Tian, S.; Ji, R.; Liu, L.; Wang, X.; Zhang, Z. Effect of water-washing on the co-removal of chlorine and heavy metals in air pollution control residue from MSW incineration. *Waste Manage.* **2017**, *68*, 221–231.
- (24) Martin, L. H. J.; Winnefeld, F.; Tschopp, E.; Müller, C. J.; Lothenbach, B. Influence of Fly Ash on the Hydration of Calcium Sulfoaluminate Cement. *Cem. Concr. Res.* **2017**, *95*, 152–163.
- (25) Zhang, S.; Wang, R.; Xu, L.; Hecker, A.; Ludwig, H. M.; Wang, P. Properties of Calcium Sulfoaluminate Cement Mortar Modified by Hydroxyethyl Methyl Celluloses with Different Degrees of Substitution. *Molecules* **2021**, *26*, 2136.
- (26) Skibsted, J.; Snellings, R. Reactivity of supplementary cementitious materials (SCMs) in cement blends. *Cem. Concr. Res.* **2019**, *124*, No. 105799.
- (27) Trincal, V.; Thiéry, V.; Mamindy-Pajany, Y.; Hillier, S. Use of hydraulic binders for reducing sulphate leaching: application to gypsiferous soil sampled in Ile-de-France region (France). *Environ. Sci. Pollut. Res.* **2018**, *25*, 22977–22997.
- (28) Sadique, M.; Al-Nageim, H.; Atherton, W.; Seton, L.; Dempster, N. Analytical investigation of hydration mechanism of a non-Portland binder with wastepaper sludge ash. *Constr. Build. Mater.* **2019**, *211*, 80–87.
- (29) Bolaños-Vásquez, I.; Trauchessec, R.; Tobón, J. I.; Lecomte, A. Influence of the ye'elimite/anhydrite ratio on PC-CSA hybrid cements. *Mater. Today Commun.* **2020**, *22*, No. 100778.
- (30) Bizzozero, J.; Gosselin, C.; Scrivener, K. L. Expansion mechanisms in calcium aluminate and sulfoaluminate systems with calcium sulfate. *Cem. Concr. Res.* **2014**, *56*, 190–202.
- (31) Le Saoût, G.; Lothenbach, B.; Taquet, P.; Fryda, H.; Winnefeld, F. Hydration of calcium aluminate cement blended with anhydrite. *Adv. Cem. Res.* **2018**, *30*, 24–36.
- (32) Rungchet, A.; Poon, C. S.; Chindaprasirt, P.; Pimraksa, K. Synthesis of Low-Temperature Calcium Sulfoaluminate-Belite Cements from Industrial Wastes and Their Hydration: Comparative Studies between Lignite Fly Ash and Bottom Ash. *Cem. Concr. Compos.* **2017**, *83*, 10–19.
- (33) Mrak, M.; Winnefeld, F.; Lothenbach, B.; Dolenc, S. The Influence of Calcium Sulfate Content on the Hydration of Belite-Calcium Sulfoaluminate Cements with Different Clinker Phase Compositions. *Mater. Struct.* **2021**, *54*, 212.
- (34) Luo, Z. T.; Ma, B. G.; Yu, Z. Q. Influence of heavy metal Pb on hydration and leaching toxicity of sulfoaluminate cement. *J. Qingdao Technol. Univ.* **2009**, *30*, 130–133.
- (35) Liu, W.; Teng, L.; Rohani, S.; Qin, Z.; Zhao, B.; Xu, C. C.; Liang, B.; et al. CO<sub>2</sub> Mineral Carbonation Using Industrial Solid Wastes: A Review of Recent Developments. *Chem. Eng. J.* **2021**, *416*, No. 129093.
- (36) Roychand, R.; Li, J.; Kilmartin-Lynch, S.; Saberian, M.; Zhu, J.; Youssf, O.; Ngo, T. Carbon Sequestration from Waste and Carbon Dioxide Mineralisation in Concrete—A Stronger, Sustainable and Eco-Friendly Solution to Support Circular Economy. *Constr. Build. Mater.* **2023**, *379*, No. 131221.
- (37) Van Gerven, T.; Van Keer, E.; Aricx, S.; Jaspers, M.; Wauters, G.; Vandecasteele, C. Carbonation of MSWI-bottom ash to decrease heavy metal leaching, in view of recycling. *Waste Manage.* **2005**, *25*, 291–300.
- (38) Baciocchi, R.; Costa, G.; Lategano, E.; Marini, C.; Poletti, A.; Pomi, R.; Postorino, P.; Rocca, S. Accelerated carbonation of different size fractions of bottom ash from RDF incineration. *Waste Manage.* **2010**, *30*, 1310–1317.
- (39) Ashraf, M. S.; Ghoul, Z.; Shao, Y. Production of Eco-Cement Exclusively from Municipal Solid Waste Incineration Residues. *Resour. Conserv. Recycl.* **2019**, *149*, 332–342.
- (40) Valls, S.; Vazquez, E. Accelerated carbonation of sewage sludge–cement–sand mortars and its environmental impact. *Cem. Concr. Res.* **2001**, *31*, 1271–1276.
- (41) Venhuis, M. A.; Reardon, E. J. Vacuum method for carbonation of cementitious wasteforms. *Environ. Sci. Technol.* **2001**, *35*, 4120–4125.
- (42) Lange, L. C.; Hills, C. D.; Poole, A. B. Effect of carbonation on properties of blended and non-blended cement solidified waste forms. *J. Hazard. Mater.* **1997**, *52*, 193–212.
- (43) Bergmans, J.; Nielsen, P.; Snellings, R.; Broos, K. Recycling of Autoclaved Aerated Concrete in Floor Screeds: Sulfate Leaching Reduction by Ettringite Formation. *Constr. Build. Mater.* **2016**, *111*, 9–14.
- (44) Wang, L.; Jin, Y.; Nie, Y. Investigation of Accelerated and Natural Carbonation of MSWI Fly Ash with a High Content of Ca. *J. Hazard. Mater.* **2010**, *174*, 334–343.
- (45) Li, X.; Bertos, M. F.; Hills, C. D.; Carey, P. J.; Simon, S. Accelerated Carbonation of Municipal Solid Waste Incineration Fly Ashes. *Waste Manage.* **2007**, *27*, 1200–1206.
- (46) Auvere Power Plant. Affordable, Versatile, Sustainable. <https://www.eneft.com/technology/power-production> (accessed October 5, 2022).
- (47) Utilitas Tallinn. <https://www.utilitas.ee/en/company/as-utilitas-tallinn/> (accessed October 5, 2022).



- (48) Neo Performance Materials <https://www.neomaterials.com/> (accessed October 5, 2022).
- (49) Gorkunov, V.; Munter, R. In *Possibilities of Utilization of Waste Slags from Niobium Production*, Proceedings of International Conference: Eco-Balt' 2007, Riga, May 10–11, 2007.
- (50) Poletini, A.; Pomi, R.; Stramazzo, A. Carbon sequestration through accelerated carbonation of BOF slag: Influence of particle size characteristics. *Chem. Eng. J.* **2016**, *298*, 26–35.
- (51) Kassahun, E.; Mekuria, S.; Beyan, S. M. Specific Surface Area Enhancement of Waste Tire-Based Activated Carbon by Demineralization Technique and Adsorption of Methylene Blue. *Int. J. Chem. Eng.* **2022**, *2022*, 1–15.
- (52) Soutsos, M. N.; Tang, L. The effect of silica fume and fly ash on the hydration of calcium aluminate cement. *Cem. Concr. Res.* **2005**, *35*, 949–954.
- (53) ASTM C618: *Standard Specification for Coal Fly Ash and Raw or Calcined Natural Pozzolan for Use in Concrete* ASTM International: West Conshohocken, PA; 2012.
- (54) Van Gerven, T.; Moors, J.; Dutre, V.; Vandecasteele, C. Effect of CO<sub>2</sub> on leaching from a cement-stabilized MSWI fly ash. *Cem. Concr. Res.* **2004**, *34*, 1103–1109.
- (55) Uibu, M.; Somelar, P.; Raado, L.-M.; Irha, N.; Hain, T.; Koroljova, A.; Kuusik, R. Oil shale ash based backfilling concrete – strength development, mineral transformations and leachability. *Constr. Build. Mater.* **2016**, *102*, 620–630.
- (56) Siddique, R.; Iqbal Khan, M. Fly Ash. In *Supplementary Cementing Materials. Engineering Materials*; Springer: Berlin, 2011; Vol. 37.
- (57) Pyatina, T.; Sugama, T.; Moon, J.; James, S. Effect of tartaric acid on hydration of a sodium-metasilicate-activated blend of calcium aluminate cement and fly ash. *Materials* **2016**, *9*, 422.
- (58) Zhang, Y.; Zhang, H.; Zhang, X. Influence of calcined flue gas desulfurization gypsum and calcium aluminate on the strength and AFT evolution of fly ash blended concrete under steam curing. *Materials* **2021**, *14*, 7171.
- (59) García-Maté, M.; De la Torre, A. G.; León-Reina, L.; Aranda, M. A. G.; Santacruz, I. Hydration studies of calcium sulfoaluminate cements blended with fly ash. *Cem. Concr. Res.* **2013**, *54*, 12–20.
- (60) Scrivener, K.; Snellings, R.; Lothenbach, B. *A Practical Guide to Microstructural Analysis of Cementitious Materials*; CRC Press: Boca Raton, FL, 2016; Vol. 540.
- (61) Taylor, H. F. *Cement Chemistry*; Thomas Telford: London, 1997.
- (62) Collier, N. C.; Sharp, J. H.; Milestone, N. B.; Hill, J.; Godfrey, I. H. The Influence of Water Removal Techniques on the Composition and Microstructure of Hardened Cement Pastes. *Cem. Concr. Res.* **2008**, *38*, 737–744.
- (63) Chrysochoou, M.; Dermatas, D. Evaluation of Ettringite and Hydrocalumite Formation for Heavy Metal Immobilization: Literature Review and Experimental Study. *J. Hazard. Mater.* **2006**, *136*, 20–33.
- (64) Xu, L.; Wang, P.; Zhang, G. Formation of Ettringite in Portland Cement/Calcium Aluminate Cement/Calcium Sulfate Ternary System Hydrates at Lower Temperatures. *Constr. Build. Mater.* **2012**, *31*, 347–352.
- (65) Hou, W.; Liu, J.; Liu, Z.; He, F.; Zhu, J.; Cui, Y.; Jinyang, W. Calcium Transfer Process of Cement Paste for Ettringite Formation under Different Sulfate Concentrations. *Constr. Build. Mater.* **2022**, *348*, No. 128706.
- (66) Amathieu, L.; Touzo, B. Ettringite Binder for Dense Mortar, Comprising Calcium Sulphates and a Mineral Compound of Calcium Aluminates. U.S. Patent US20070094919A1, 2007.
- (67) Chen, B.; Horgnies, M.; Huet, B.; Morin, V.; Johannes, K.; Kuznik, F. Comparative Kinetics Study on Carbonation of Ettringite and Meta-Ettringite Based Materials. *Cem. Concr. Res.* **2020**, *137*, No. 106209.
- (68) Chung, C. W.; Lee, J. Y.; Kim, J. H. Formation of Hydroxyapatite in Portland Cement Paste. *J. Korea Inst. Build. Constr.* **2014**, *14*, 68–75.
- (69) Diamond, S. Mercury Porosimetry: An Inappropriate Method for the Measurement of Pore Size Distributions in Cement-Based Materials. *Cem. Concr. Res.* **2000**, *30*, 1517–1525.
- (70) Abell, A. B.; Willis, K. L.; Lange, D. A. Mercury Intrusion Porosimetry and Image Analysis of Cement-Based Materials. *J. Colloid Interface Sci.* **1999**, *211*, 39–44.
- (71) Cizer, Ö.; Van Balen, K.; Elsen, J.; Van Gemert, D. Real-time Investigation of Reaction Rate and Mineral Phase Modifications of Lime Carbonation. *Constr. Build. Mater.* **2012**, *35*, 741–751.
- (72) Pham, S. T.; Prince, W. Effects of Carbonation on the Microstructure of Cement Materials: Influence of Measuring Methods and of Types of Cement. *Int. J. Concr. Struct. Mater.* **2014**, *8*, 327–333.
- (73) Chen, B.; Laucks, M. L.; Davis, E. J. Carbon Dioxide Uptake by Hydrated Lime Aerosol Particles. *Aerosol Sci. Technol.* **2004**, *38*, 588–597.
- (74) Uibu, M.; Kuusik, R. Main Physicochemical Factors Affecting the Aqueous Carbonation of Oil Shale Ash. *Miner. Eng.* **2014**, *59*, 64–70.
- (75) Matschei, T.; Lothenbach, B.; Glasser, F. P. Thermodynamic Properties of Portland Cement Hydrates in the System CaO–Al<sub>2</sub>O<sub>3</sub>–SiO<sub>2</sub>–CaSO<sub>4</sub>–CaCO<sub>3</sub>–H<sub>2</sub>O. *Cem. Concr. Res.* **2007**, *37*, 1379–1410.
- (76) Nair, K. S.; Kumar, S. Sulfate Induced Heave: Addressing Ettringite Behavior in Lime Treated Soils and in Cementitious Materials, Ph.D. Thesis, Texas A&M University, 2010.
- (77) Baquerizo, L. G.; Matschei, T.; Scrivener, K. L. Impact of Water Activity on the Stability of Ettringite. *Cem. Concr. Res.* **2016**, *79*, 31–44.
- (78) Bertos, M. F.; Li, X.; Simons, S. J. R.; Hills, C. D.; Carey, P. J. Investigation of Accelerated Carbonation for the Stabilization of MSW Incinerator Ashes and the Sequestration of CO<sub>2</sub>. *Green Chem.* **2004**, *6*, 428–436.
- (79) Ptacek, C.; Blowes, D. Predicting Sulfate-mineral Solubility in Concentrated Waters. *Rev. Mineral. Geochem.* **2000**, *40*, 513–540.
- (80) Xu, L.; Wu, K.; Röbber, C.; Wang, P.; Ludwig, H. M. Influence of Curing Temperatures on the Hydration of Calcium Aluminate Cement/Portland Cement/Calcium Sulfate Blends. *Cem. Concr. Compos.* **2017**, *80*, 298–306.
- (81) Telesca, A.; Marroccoli, M.; Pace, M. L.; Tomasulo, M.; Valenti, G. L.; Monteiro, P. J. M. A Hydration Study of Various Calcium Sulfoaluminate Cements. *Cem. Concr. Compos.* **2014**, *53*, 224–232.
- (82) Pelletier-Chaignat, L.; Winnefeld, F.; Lothenbach, B.; Le Saout, G.; Müller, C. J.; Famy, C. Influence of the Calcium Sulfate Source on the Hydration Mechanism of Portland Cement–Calcium Sulphoaluminate Clinker–Calcium Sulfate Binders. *Cem. Concr. Compos.* **2011**, *33*, 551–561.
- (83) Seo, J.; Nawaz, A.; Jang, J. G.; Lee, H. K. Modifications in Hydration Kinetics and Characteristics of Calcium Aluminate Cement upon Blending with Calcium Sulfoaluminate Cement. *Constr. Build. Mater.* **2022**, *342*, No. 127958.
- (84) Xu, L.; Wang, P.; Zhang, G. Calorimetric Study on the Influence of Calcium Sulfate on the Hydration of Portland Cement–Calcium Aluminate Cement Mixtures. *J. Therm. Anal. Calorim.* **2012**, *110*, 725–731.
- (85) Irha, N.; Uibu, M.; Jefimova, J.; Raado, L.-M.; Hain, T.; Kuusik, R. Leaching Behaviour of Estonian Oil Shale Ash-based Construction Mortars. *Oil Shale* **2014**, *31*, 394.
- (86) Nawaz, M.; Indraratna, B.; Sivakumar, M. Geopolymers in construction - recent developments. *Constr. Build. Mater.* **2020**, *260*, No. 120472.
- (87) Ragipani, R.; Escobar, E.; Prentice, D. P.; Bustillos, S.; Simonetti, D. A.; Sant, G.; Wang, B. Selective sulfur removal from semi-dry flue gas desulfurization coal fly ash for concrete and carbon dioxide capture applications. *Waste Manage.* **2021**, *121*, 391–403.
- (88) Srivastava, S.; Snellings, R.; Cool, P. Clinker-free Carbonate-bonded (CFCB) Products Prepared by Accelerated Carbonation of

Steel Furnace Slags: A Parametric Overview of the Process Development. *Constr. Build. Mater.* **2021**, *303*, No. 124556.

(89) Mo, L.; Zhang, F.; Deng, M. Mechanical Performance and Microstructure of the Calcium Carbonate Binders Produced by Carbonating Steel Slag Paste under CO<sub>2</sub> Curing. *Cem. Concr. Res.* **2016**, *88*, 217–226.

(90) Li, N.; Mo, L.; Unluer, C. Emerging CO<sub>2</sub> Utilization Technologies for Construction Materials: A Review. *J. CO<sub>2</sub> Util.* **2022**, *65*, No. 102237.

(91) Wei, Z.; Wang, B.; Falzone, G.; La Plante, E. C.; Okoronkwo, M. U.; She, Z.; et al. Clinkering-free Cementation by Fly Ash Carbonation. *J. CO<sub>2</sub> Util.* **2018**, *23*, 117–127.

(92) Meng, J.; Liao, W.; Zhang, G. Emerging CO<sub>2</sub>-mineralization Technologies for Co-utilization of Industrial Solid Waste and Carbon Resources in China. *Minerals* **2021**, *11*, 274.

(93) Zhang, S.; Ghouleh, Z.; Shao, Y. Green Concrete Made from MSWI Residues Derived Eco-cement and Bottom Ash Aggregates. *Constr. Build. Mater.* **2021**, *297*, No. 123818.

(94) Kaliyavaradhan, S. K.; Ling, T. C.; Mo, K. H. Valorization of Waste Powders from Cement-concrete Life Cycle: A Pathway to Circular Future. *J. Cleaner Prod.* **2020**, *268*, No. 122358.